Classical and Quantum Gravity

PAPER

OPEN ACCESS

RECEIVED
30 September 2025

REVISED
15 January 2026

ACCEPTED FOR PUBLICATION
4 March 2026

PUBLISHED
7 April 2026

Evaluation of the tilt to length coefficient induced by wavefront error for the LISA interferometric test bench

Maxime Vincent[1,2,*], **Romain Arguel**[2] **and Hubert Halloin**[1]

[1] Université Paris Cité, CNRS, Astroparticule et Cosmologie (APC), F-75013 Paris, France
[2] Centre National d'Études Spatiales (CNES), Toulouse, France
[*] Author to whom any correspondence should be addressed.

E-mail: mvincent@apc.in2p3.fr

Keywords: laser interferometer space antenna, tilt to length, optical simulation

Abstract

Space-based gravitational wave detectors can be limited by a noise source arising from the coupling between interferometric beam jitter and the interferometer's length readout. A significant optical property responsible for this coupling is the wavefront error, defined as distortions in the phase profile of the laser beam. In this paper, we investigate this tilt to length (TTL) coupling induced by wavefront errors by developing two independent simulation tools that employ different computational methods to quantify the coupling amplitude. We analyze the characteristics of distortion-induced TTL coupling and present the relationship between the magnitude of wavefront distortions—expressed through a Zernike polynomial decomposition—and the resulting coupling amplitude. These results provide critical specifications for the design of an optical test bench intended to experimentally verify the performance of the laser interferometer space antenna instrument on ground.

1. Introduction

Space-based gravitational wave detectors offer the unique opportunity to observe low frequency gravitational waves in the millihertz band, a region inaccessible to ground-based observatories due to seismic noise [1]. The laser interferometer space antenna (LISA), currently in its detailed design phase and coordinated by the European Space Agency, is a space-based observatory designed to detect gravitational waves in the millihertz band. LISA will consist of three spacecraft roughly forming a equilateral triangle with an arm length of 2.5 million kilometers using heterodyne interferometry to measure distance variations between the spacecraft test masses serving as geodesic [2]. The interferometric core of LISA is composed of three interferometers [1]: the reference interferometer (used as a stable phase reference), the test mass interferometer (used to measure the relative position between the geodesic test mass reference housed inside the spacecraft and the spacecraft itself, thereby allowing suppression of the spacecraft's motion [3]) and the science interferometer (used for the measurement between two spacecraft). To verify that LISA will be able to reach it is scientific goals, a complex test set up is being developed to characterize and validate the performance of the optical metrology system on ground.

A potentially critical noise source specific to interferometric systems like LISA arises from the coupling between the relative jitter of the laser beams and the optical path length[3] readout of the interferometer [4]. The relative motion between spacecrafts, combined with pointing fluctuations, will induce variations in the optical path length measurement that will lead to excess noise in the measurement in the form of a pseudo-length signal. This residual jitter couples with the interferometric read out yielding the distance measurement, thus reducing the performance of the instrument. This coupling is

[3] Optical path length (OPL) is defined as the geometrical distance that the beam travels multiplied by the refraction index of the media of propagation.

known as tilt to length (TTL) coupling and is one of the limiting instrumental noise of LISA, TTL is expressed in units of longitudinal length variation per unit angle[4]. This effect is highly dependent on the interferometer optical design and properties, it must be modeled and characterized in order to reach the expected performance of the instrument.

This coupling can be decomposed in two types: geometric [5] and non-geometric [6]. The geometric component originates from direct modifications in the optical path induced by beam tilts, introducing phase shifts that will increase the noise of the measurement. This occurs when angular misalignments lead to variations in the effective optical path sensed by the interferometer [5]. On the other hand, any change in the measured optical path length due to a relative angle between the interfering beams, that do not originate from direct geometric changes in the optical path, is classified as non geometric TTL coupling [6]. Non-geometric TTL can arise from several mechanisms, including mismatches in the wavefront curvature of the interfering beams, misalignment of their barycenters on the detector, or the presence of optical aberrations and wavefront distortions. This latter mechanism is the primary focus of this study.

TTL can be mitigated through careful optical design, such as the use of imaging systems that minimize beam walk at the detector [7]. In addition, post-processing correction is possible if the relative angle between interfering beams is known and the corresponding TTL coupling coefficient has been accurately calibrated in orbit [8]. The relative angle between beams is measured using quadrant photoreceivers, whose active surfaces are divided into four independent segments. By comparing the optical phase across the quadrants, the wavefront tilt and thus the angle between the interfering beams—can be reconstructed with high precision [9].

Wavefront error (WFE)[5] can induce a TTL coupling by breaking the symmetry of the phase integration over the photoreceiver surface. In the ideal case of two identical, aberration-free plane wavefronts, a relative tilt between the beams (when the rotation pivot is at the center of the photoreceiver sensing plane) produces opposite phase shifts on opposite sides of the detector. While each quadrant individually experiences a non-zero phase change, these contributions are antisymmetric. When summed over all four quadrants to compute the total optical pathlength signal, the positive and negative phase contributions cancel. The total pathlength signal thus remains unchanged with respect to the untitled case. This cancellation no longer holds when WFE is present on one of the beams. In that case, the phase distribution across the photoreceiver becomes asymmetric, and the phase contributions from different quadrants no longer sum to zero. A relative beam tilt can then induce not only a differential phase between quadrants, but also a residual common-mode phase shift. This common-mode component does not cancel in the total OPL signal and manifests as an apparent pathlength change, even though it originates purely from angular motion. Consequently, WFE can convert beam tilts into unwanted optical pathlength noise through TTL coupling.

The first part of this paper introduces the test setup being developed to test and validate the performance of the interferometric core of LISA. The second part will present two simulation tools developed, aimed at quantifying different sources of TTL. Finally, an application of these tools is shown through a study of wavefront error effects on TTL coupling, including a comparison between the two simulation approaches.

2. Interferometric detection system (IDS) test set-up

In the framework of the LISA project, the IDS corresponds to the metrological core of the instrument, namely the optical bench (including pointing mechanisms and photoreceivers), the signal measurement unit (phasemeter) and the optical bench main control unit. The main function of the IDS is to measure, using high stability heterodyne interferometry, the relative phase and orientation between the transmitted laser and the received beam coming from the distant satellite (after collimation by a telescope), and between the transmitted laser and a local laser after reflection on the inertial test mass [1]. The IDS is set and specified to be able to reach a measurement noise floor of about $10\,\mathrm{pm}/\sqrt{\mathrm{Hz}}$. The French LISA community is developing the ground support equipment and test benches to conduct the functional and performance validation for the IDS.

In order to be tested on ground, the optical bench is surrounded by two additional benches simulating the optical interfaces with the telescope and with the test mass:

[4] $\mathrm{TTL}(\theta) = \frac{\mathrm{dOPL}}{\mathrm{d}\theta}$ with θ the angle between interfering beams.

[5] WFE: deviation of the wavefront phase from an ideal wavefront. It can be introduced by any optical element along the beam path, whether in transmission or reflection. It is commonly described using Zernike polynomials [10], an orthogonal set of functions forming a basis on the unit circle.

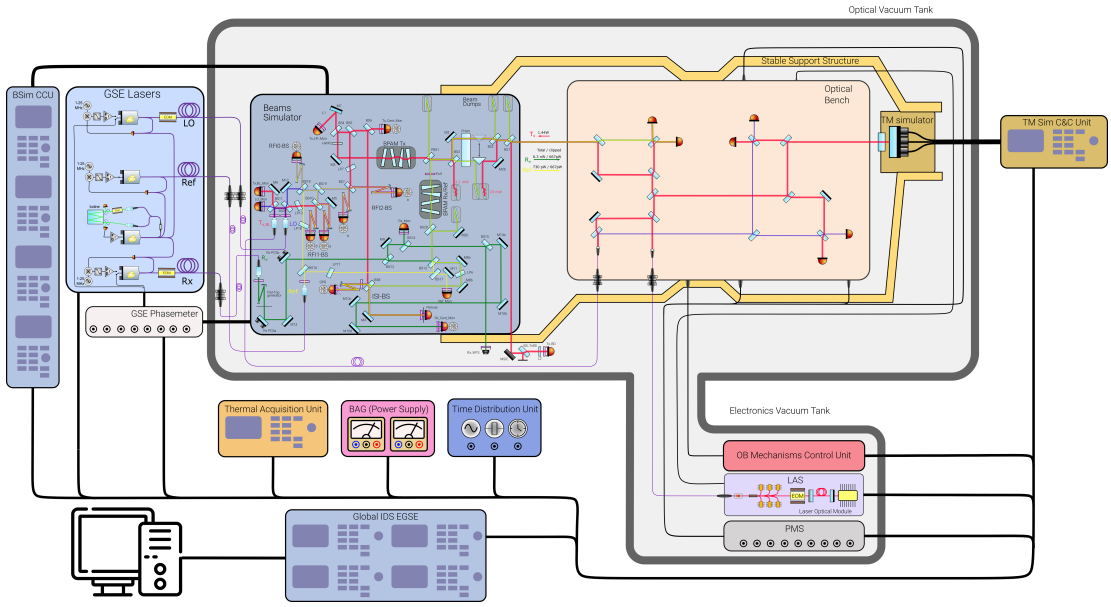

Figure 1. Simplified schematic representation of the Interferometric Detection System Test Set Up.

- The 'beams simulator' (figure 1) (BSim): simulates the telescope interface receiving (and emitting) the beam from the distant spacecraft. This bench is the main object of the present study.
- The 'test mass simulator' (figure 1): simulates the interface with the test mass. It is essentially a tip tilt and piston driven mirror with picometer stability and high actuation resolution requirements.

The main requirements governing the design of the BSim are the following:

- Measurement of the noise floor of the Science Interferometer (figure 1). The test setup is designed to contribute no more than $10\,\mathrm{pm}/\sqrt{\mathrm{Hz}}$ to the measurement in the frequency band from 30 mHz to 1 Hz, in compliance with the IDS noise requirements and to represent the contribution of the corresponding unit on the distant spacecraft. The BSim is thus equipped with an interferometer called ISI BS (i.e. inter-spacecraft interferometer (figure 1)) to act as the other half of the Science interferometer on the distant spacecraft.
- Generation of a flat top beam representative of the distant beam collimated and clipped by the telescope. A beam expander and petal shaped apodization mask [11] allows for the generation of a 10 mm diameter beam with a useful 'high quality' diameter of 2.5 mm. The apodization aperture (see figure 2) follows a radial intensity transmission profile described by a hyper Gaussian function:

$$\mathrm{HG}(\rho,a,b,n)=\begin{cases}1, & \text{if } \rho\leqslant a,\\ \exp\left[-\left(\frac{\rho-a}{b}\right)^{n}\right], & \text{if } \rho>a\end{cases} \tag{1}$$

  with ρ the radius position on the aperture, a the inner radius of hyperGaussian, b the $1/e^n$ attenuation length and n its order.
- Measurement of the TTL coefficient of the science interferometer at the center of the entrance pupil of the OB, which is conjugated with the photoreceivers of the science interferometer, with a maximum error induced by the test set up of $15\,\mu\mathrm{m\,rad}^{-1}$ at a 99.7% (i.e. $3\,\sigma$ confidence interval for a normally distributed error).

Since the measurement of the TTL coupling coefficient is split between the two optical benches, the intrinsic contribution of the test equipment must be both well understood and minimized. In particular, the geometric component of TTL generated within the test bench must be effectively suppressed. Otherwise, angular actuation of the flat–top beam would introduce a dominant and indistinguishable contribution from the test setup itself, preventing compliance with the requirement that the test-equipment TTL contribution remain below $15\,\mu\mathrm{m\,rad}^{-1}$. To suppress this effect, the flat–top beam is phase-locked to an auxiliary reference beam that is not affected by the angular actuation. The photoreceptor used for this phase lock is located at an optical copy of the interface with the optical bench

(i.e. at the rotation pivot point located at the OB pupil) on the BSim bench. As a result, all phase fluctuations induced by actuating the flat top beam are absorbed by the phase locking loop, thus canceling the geometric TTL contribution originating from the test setup.

To prevent wavefront error induced biases in the phase locking signal, the lock is performed using the phase measured by a pinhole photo receiver centered on the rotation pivot point. The pinhole acts as a spatial filter, ensuring that the phase is measured locally at the pivot. While a smaller pinhole improves the approximation of an ideal pivot point measurement, it also reduces the available optical power. Dedicated studies were therefore carried out to quantify the impact of the pinhole diameter on wavefront induced TTL coupling, allowing for a trade off between incident flux and acceptable residual TTL coupling.

A control loop acting on the actuators steering the flat top beam is used to maintain the beam centered on the predefined rotation pivot point at the optical bench pupil, and consequently on the photo receivers. This ensures that beam rotation effectively occurs about the photo receiver surface center.

The non-geometric component of TTL coupling cannot be suppressed. As in any complex optical system, the large number of optical elements on the bench and the generation of the flat top beam will introduce some wavefront distortion. The only way to control this contribution is to understand the coupling amplitude induced by a given amount of distortion on the beam. This knowledge enables the derivation of acceptable wavefront error budgets, both for individual optical components and for the BSim as a whole.

To establish these specifications, two dedicated simulation tools were developed to quantify the TTL coupling induced by various wavefront aberrations introduced along the beam path, with two different techniques. One was developed by AstroParticule et Cosmology laboratory (APC) and the second tool was developed by the centre national d'etudes spatiales(CNES).

3. Optical simulations

The APC code developed in the framework of this study was designed as a modular simulation tool, easily adaptable to various physical situations, including the analysis of wavefront error effects. It was also used to investigate the influence of specific stray-light sources on TTL coupling. The core of the simulation tool is based on the PROPER Python library [12], a physical optics propagation package that models the propagation of electromagnetic fields using Fourier-based algorithms, including the angular spectrum method [13] and Fresnel approximations [13]. The choice of method depends on the propagation distance and simulation parameters, enabling both near-field and far-field modeling. While physical propagation is computationally expensive, requiring high-resolution sampling over large simulation grids to mitigate boundary effects, it offers the advantage of including diffraction and propagation-induced modifications to the wavefront. It also allows for the accurate simulation of diffraction patterns from complex aperture shapes, such as the apodization masks used to generate the flat top beam (see figure 2).

The basis of this simulation tool is to generate two laser beams and propagate them to a detector, while having the possibility of adding apertures between the beam source and the detector and imposing a lateral shift on one of the beams or detector. The wavefront amplitude and phase, aperture shapes and detector geometry, are user-defined. With these basic building blocks in place, additional physical effects can easily be added by inserting corresponding Python routines between the simulation stages. For example, to simulate a flat–top beam, an apodization aperture can be placed after the generation of a large Gaussian beam. The beam is then propagated through the aperture to accurately model the flat–top intensity profile that will be generated on the BSim. Similarly, to introduce a tilt to the incoming beam, a linear phase ramp can be added to the wavefront at the end of the propagation step to simulate the tilt on the surface of the photo receiver. This approach is consistent with the physical configuration, in which a control loop maintains the beam centered on the rotation pivot point, and imaging systems ensure proper beam centering on the photo receivers. To simulate an angular actuation sequence, the wavefront can be duplicated n times, with the corresponding tilt phase map applied to each copy.

This yields a simple TTL simulation tool, which main steps are:

1. Generate two laser beams with a phase and intensity profile of the user's choice
2. Propagate both fields at a given distance
3. Apply tilt to one of the two beams
4. Repeat step 3. for a series of tilt angles to create the angular actuation
5. Shift the beam laterally (optional)

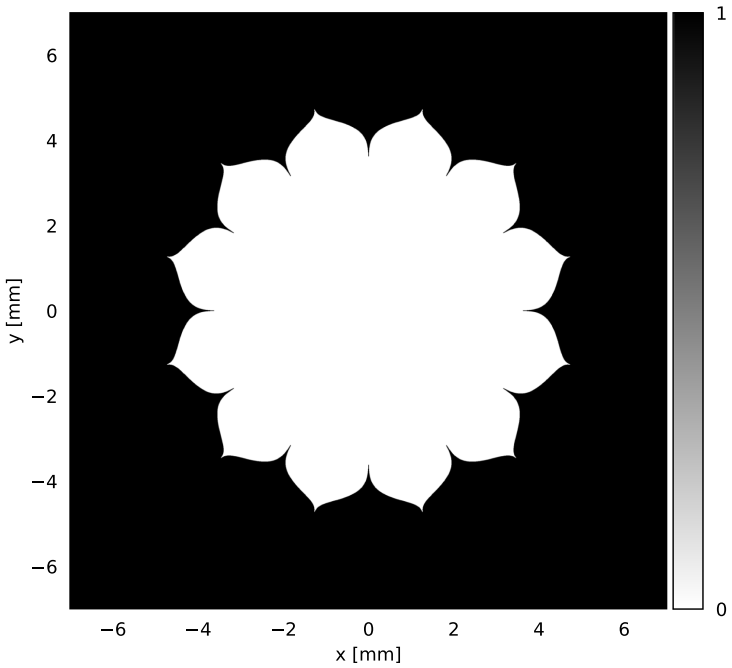

Figure 2. Opacity map of the hyperGaussian apodization mask used for flat–top beam generation. An opacity of 0 corresponds to full transmission, while 1 corresponds to complete blocking. The hyperGaussian parameters are $a = 0.2$, $b = 0.25$, $n = 12$ and 12 petals.

6. Apply a detector mask (usually, a quadrant photo-receiver) and optionally shift the mask laterally
7. Compute the interference between each tilted beam and the reference (untilted) beam, the phase of the detector is defined in this study as the mean value of the individual phases of the four quadrants[6].
8. Extract the phase difference (i.e. the optical pathlength difference from an actuation at angle θ_j to the next actuation angle θ_{j+1}) as a function of tilt angle and derive the corresponding TTL coupling coefficient. The coupling coefficient values presented in this paper correspond to the maximum coupling observed over the entire actuation range $[-300, +300]$ μrad , and are defined as:

$$\mathrm{TTL} = \max_j \left| \frac{\mathrm{OPL}\left(\theta_{j+1}\right) - \mathrm{OPL}\left(\theta_j\right)}{\theta_{j+1} - \theta_j} \right|. \tag{2}$$

This definition ensures that potential biases arising from asymmetric wavefront error distribution, particularly those that would shift the coupling coefficient minimum away from the center of the actuation range, are eliminated.

In order to study the coupling induced by wavefront distortion, an error map can be added between step 2 and 3 without further adjustment. Due to the manufacturing and polishing processes of optical surfaces, a wide variety of wavefront error distributions can arise. Consequently, optical surface quality is often specified in terms of the root-mean-square (RMS) wavefront distortion on a given surface. A statistical analysis, with a large number of different wavefront error distributions, is thus required to be able to confidently specify the optical quality of the system as a whole. To implement this, a loop is added on steps 3 to 7 to calculate the TTL coupling coefficients for a large set of different wavefront error distributions. To generate these maps we chose to perform the study using Zernike polynomials [10] up to Noll classification [14] index 36 while excluding order 1, 2 and 3 corresponding to piston and tip tilt modes. The piston represents a uniform phase offset and does not contribute to differential optical pathlength measurements. Tip tilt modes are formally equivalent to an angular misalignment of the beam and are therefore already included in the TTL study.

The map generation procedure is as follows:

[6] Other formalisms of the reconstruction of optical pathlength from the photodetector signals exists and can have an influence on the retrieved signals, a study of the influence of this formalism on the coupling can be found in [6].

Table 1. General simulation parameters for APC and CNES simulations.

Parameter	APC tool	CNES tool
Detector radius	1.12×10^{-3} m	1.12×10^{-3} m
QPD dead zone size	30×10^{-6} m	20×10^{-6} m
Wavelength	1064×10^{-9} m	1064×10^{-9} m
Gaussian beam waist radius	1.12×10^{-3} m	1.25×10^{-3} m
Flat top beam radius	$\sim 5 \times 10^{-3}$ m	1.25×10^{-3} m
Apodization mask radius	$\sim 5 \times 10^{-3}$ m	NA
Gaussian beam propagation distance	1 m	NA
Flat top beam propagation distance	1 m	NA
TTL actuation range	$\pm 300\ \mu$rad	$\pm 300\ \mu$rad
TTL actuation direction	horizontal and/or vertical	horizontal and/or vertical

Note: The dead zone of a quadrant photoreceiver corresponds to the spacing between the quadrants of the photoreceiver that are not sensitive to light.

1. Each Zernike polynomial is assigned a coefficient c_i, randomly drawn from a uniform probability distribution over the interval $[-1, +1]$.
2. Each coefficient c_i is then multiplied by a weighting factor w_i.
3. The quadratic sum of the weighted coefficients, from Noll index 4 to 36 , is computed in order to normalize the overall wavefront error to the desired wavefront error RMS value (in unit meters). The final coefficient C_i associated with the Zernike polynomial of order i is thus given by:

$$C_i = c_i \cdot w_i \cdot \frac{\mathrm{WFE_{RMS}}}{\sqrt{\sum_{j=4}^{36} \left(c_j w_j\right)^2}} \quad \text{with } w_i = A\mathrm{e}^{-Bi}. \tag{3}$$

The weighting function w_i commonly used in this study follows a decreasing exponential law, which emphasizes lower-order aberrations typically found in optical surfaces. This exponential behavior was empirically adjusted to match wavefront error distribution observed in optical surfaces with classical polishing processes ($A = 1.24$ and $B = 0.06$). Uniform weighting functions were also tested to evaluate the sensitivity of the coupling to the shape of the weighting law.

The second simulation tool was developed in parallel to this study by the CNES, with the goal of cross-checking results and increasing confidence in the validity of both tools. This tool is solely based on gaussian geometric optics, the wavefront is modeled directly at the detector surface. The wavefront is tilted and then projected on the surface of the detector before adding a wavefront error map and computing the interference with the other beam. Thus the propagation and diffraction effects are not taken into account with this tool. The same procedure is used for the generation of the wavefront error maps and characteristics of both simulations can be found in table 1. The flat top used in this simulation is a perfect ideal flat wavefront. This tool was partly inspired by an existing simulation library 'Fieldprop' developed for similar purposes in the context of LISA flight hardware simulation by E. Fitzsimons (UK Astronomy Technology Center, Royal Observatory Edinburgh). Some differences between the two models arise from technical considerations, such as the different dead zone sizes implemented in each model. Achieving proper sampling of a smaller dead zone requires an increased spatial resolution, which in turn leads to a significant increase in computation time in the APC tool due to the use of Fourier transform propagation. Additional discrepancies also stem from the propagation methods themselves. In the APC tool, the flat top beam is generated by propagating a Gaussian beam through the apodization mask, resulting in a flat top intensity profile together with the associated diffraction features. In contrast, the CNES tool models the flat top beam as an ideal flat wavefront, without diffraction effects.

4. Results

To establish a baseline understanding of how wavefront aberrations contribute to TTL coupling in the experimental set up described above, an initial set of simulations was carried out. The study first examined the influence of individual Zernike polynomials to identify which orders were the main contributors to the coupling. The linearity and additivity of the TTL response were then investigated to assess the superposition behavior of multiple aberrations. Building on these results, a statistical analysis was performed using a large array of wavefront aberration distributions, with the goal of defining optical quality specifications for the BSim.

Table 2. Zernike polynomial terms that generate significant TTL coupling for an actuation on the horizontal or vertical axis.

Noll index	Corresponding aberration
4	Defocus
6	Primary astigmatism
11	Primary spherical aberration
12	Secondary astigmatism
14	Quadrafoil
22	Secondary spherical aberration
24	Tertiary astigmatism
26	Tertiary quadrafoil
28	Tertiary hexafoil

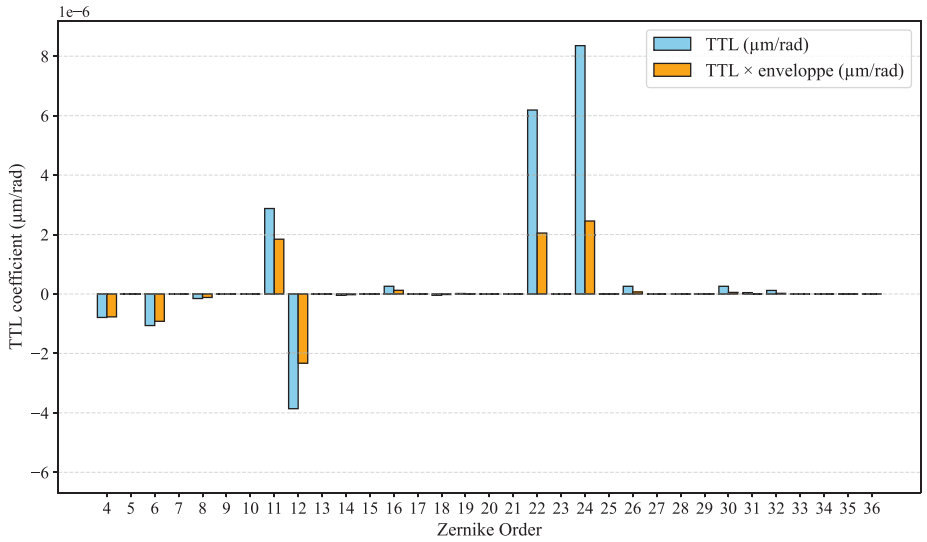

Figure 3. Coupling coefficients of individual Zernike modes for horizontal angular actuation. Also shown is the distribution corrected by the weighting function defined in equation (3).

4.1. Influence of individual Zernike polynomials

To evaluate the influence of each Zernike polynomial order on TTL coupling, simulations were done using both tools. For each order, a fixed wavefront error was added exclusively to that Zernike mode in the phase profile. The added error was normalized for consistency to an rms wavefront error of 35 nm RMS[7], even if high order modes tend to have smaller amplitude in real optical systems. The actuation was applied in both directions associated to QPD axis (horizontal and vertical) with beams remaining perfectly centered on the detector. Zernike orders from 4 (defocus) to 36 (heptafoil) were investigated. The results, summarized in table 2, lists only the dominant TTL-generating modes for both horizontal and vertical angular actuation. Both tools show good agreement for these main contributors. Figure 3 shows the coupling coefficients for each Zernike order for a wavefront error amplitude of 35 nm RMS considering an horizontal angular actuation. The figure also displays the same distribution after application of the weighting function defined in equation (3), highlighting how the contribution to the coupling of high Zernike order modes is reduced by the weighing function to better reflect realistic optical systems. Since the beams intensity profiles considered here are perfectly symmetric and centered on the QPD active area, the ability to generate non-geometrical TTL effects only depends on the symmetry properties of the WFE. By definition, the individual Zernike terms exhibits either central symmetry or antisymmetry.

On one hand, it can be verified that antisymmetric profiles are not able to produce any non-geometrical TTL, since two diametrically opposite points on the detector will contribute to the overall phase in completely opposite ways during angular actuation, which will ultimately results in total cancellation of the phase angular dependency. On the other hand, symmetric profiles always have the "potential" to generate some TTL, provided that the considered actuation axis is not oriented along one

[7] Corresponding to $\lambda/30$, initial coarse estimate of the wavefront quality needed to reach the performance specified for the TTL measurement.

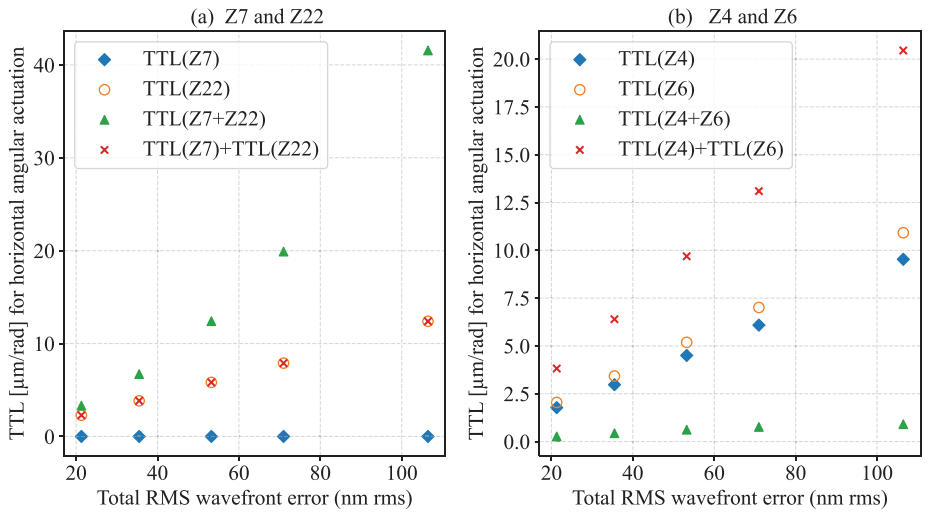

Figure 4. Illustration of TTL non-additivity: comparison between the TTL induced by individual Zernike modes and by their combination.

antisymmetric axis that some of those Zernike terms can exhibit. In our example, Zernike terms with Noll indices 5, 13, 15, 23, 25, and 27 are symmetric but fail to meet this condition: they correspond to the same basic symmetric structure as terms 6, 12, 14, 24, 26, and 28, but with an azimuthal rotation that introduces asymmetry along the TTL actuation axis. Nevertheless, these profiles remain potential TTL generators for a suitably oriented actuation axis.

4.2. Additivity and linearity of TTL

A realistic wavefront is described by a linear combination of Zernike modes rather than a single polynomial. As expected for a phase-induced coupling, the TTL coupling exhibits nonlinear behavior, as previously shown for the LISA long-arm interferometer [15] and confirmed by simulations of our system. Two key properties were investigated:

- **Non-additivity:**

$$\mathrm{TTL}\left(\mathrm{WFE}_1 + \mathrm{WFE}_2\right) \neq \mathrm{TTL}\left(\mathrm{WFE}_1\right) + \mathrm{TTL}\left(\mathrm{WFE}_2\right). \tag{4}$$

- **Non-homogeneity:**

$$\mathrm{TTL}\left(\alpha \cdot \mathrm{WFE}\right) \neq \alpha \cdot \mathrm{TTL}\left(\mathrm{WFE}\right), \quad \alpha \in \mathbb{R} \tag{5}$$

Figure 4 illustrates this behavior. In figure 4(b), the TTL response of the combined Z_4 (defocus) and Z_6 (vertical astigmatism) modes differs significantly from the sum of their individual contributions. Although absolute coupling values are shown, both modes contribute with the same sign (see figure 3). An even stronger effect is observed when combining a TTL generating mode with a non generating one: figure 4(a) shows that while Z_7 (vertical coma) alone produces negligible TTL, its combination with Z_{22} (secondary spherical) leads to a significant increase in coupling. This demonstrates that non-generating modes can become effective TTL contributors in the presence of other aberrations. These results show that single-mode analyses are insufficient and may lead to under or overestimation of TTL. Consequently, a statistical approach based on a large ensemble of randomly generated wavefront error maps is required to derive reliable optical quality specifications for the BSim.

4.3. WFE induced TTL coupling

Based on the results presented above, it becomes essential to simulate a large number of randomly generated wavefront error maps. In the present study, for each WFE RMS amplitude, 1000 maps were generated using the generation procedure described in (1). Analyzing the distribution and amplitude of the resulting TTL coefficients for a fixed RMS wavefront error allows for the determination of a maximum coupling value at a given confidence level on the set that was studied. It should be noted that not all 32 Zernike modes considered act as significant TTL generators: in practice, only a subset of modes contributes significantly to the coupling, while most modes have negligible effect individually. However, as

Table 3. Wavefront error simulation parameters for APC and CNES simulations.

Parameter	APC tool	CNES tool
Wavefront error RMS amplitude on application zone	$\lambda/10$, $\lambda/15$, $\lambda/20$, $\lambda/30$, $\lambda/50$, $\lambda/100$	$\lambda/10$, $\lambda/15$, $\lambda/20$, $\lambda/30$, $\lambda/50$, $\lambda/100$
Zernike coefficients applied	4 to 36	4 to 36
RMS per Zernike coefficient	Normalized random draw	Normalized random draw
WFE application diameter	$2,74 \cdot 10^{-3}$ m	$2,24 \cdot 10^{-3}$ m

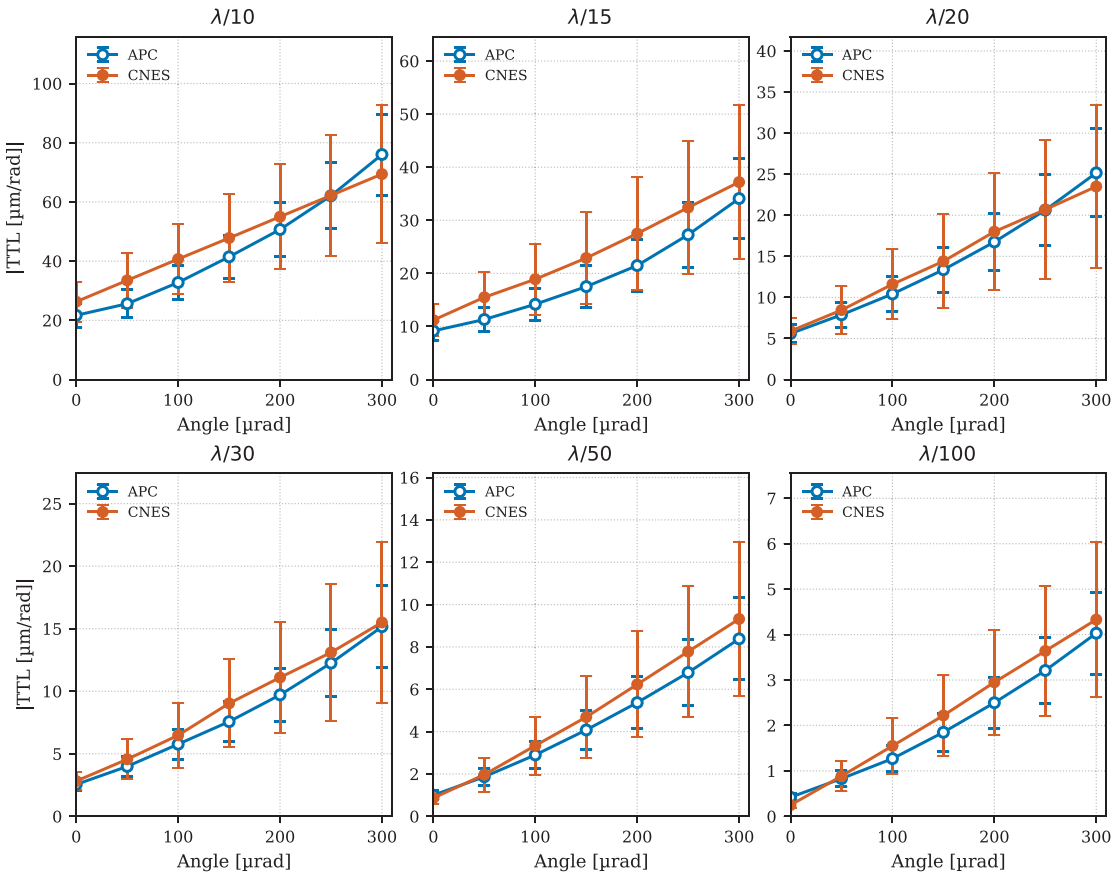

Figure 5. TTL coupling as a function of actuation angle for various wavefront error levels. Results are given at 99.7% confidence level interval.

observed in the previous section, some non-generating modes can produce TTL when combined with generators. Given this, the 1000 randomly generated WFE maps used in our simulations were deemed sufficient to capture the main TTL behavior, providing a representative estimate of the 99.7% confidence interval for our simulation parameters and experimental setup. Extreme combinations of weak or non generating modes could lead to slightly higher or lower TTL, but are unlikely. In order to be representative of the system for which specifications are being written, the simulation parameters have been adapted to the optical test bench being developed for LISA. The general simulation parameters can be found in table 1 and the WFE specific parameters in table 3.

Figure 5 presents the results of simulations performed with wavefront error amplitudes ranging from 10.64 nm to 106.4 nm rms (corresponding to $\lambda/100$ to $\lambda/10$) for maps generated using the exponential distribution previously described. The reported coupling coefficient represents the 99.7% confidence level interval of |TTL|. For reference, the standard deviation of the same quantity is represented as error bars. Both simulation tools yield consistent results, with the APC tool systematically producing slightly lower TTL values compared to the CNES tool. This discrepancy arises primarily from differences in the implementation of certain simulation parameters inherent to each tool. The most significant differences concern the detector geometry and implementation—linked to spatial resolution constraints—and the flat–top beam modeling, which, in the APC tool, accounts for diffraction effects and the residual Gaussian curvature of the beam profile along with the propagation effects. A set of simulations was

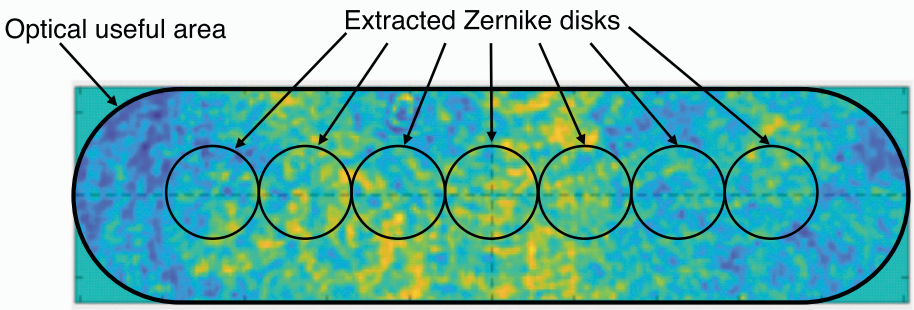

Figure 6. Surface quality map of a 25 mm × 5 mm optical interface showing the extracted disks used for the TTL simulation.

also performed by introducing wavefront errors on the Gaussian reference beam in addition to the initially distorted flat–top beam. This approach assumed that the two wavefront error distributions were uncorrelated (i.e. both beams passed though different optics). The CNES simulation tool yielded a TTL coupling coefficient higher by a factor of $\sim\sqrt{2}$ at a 68.2 % confidence level, while the APC tool produced a coefficient higher by a factor of $\sim\sqrt{2}$ at the 98 % confidence level. This outcome aligns with the expected result for the combination of two uncorrelated wavefront error sources. The equivalent simulation performed with a uniform weighting function[8] yielded slightly higher TTL coupling coefficients. This is explained by the fact that, under such a distribution, high Zernike order generator terms are assigned greater amplitudes compared to those in a decreasing exponential distribution. However, in practice, optical surface polishing processes tend to induce the presence of low spatial frequency aberrations, making the exponential weighting a more realistic representation of typical surface errors.

Another set of simulations were then performed using a set of measured wavefront error maps obtained from a previously developed optical interferometry demonstrator bench [16]. The optical components of this bench are representative of those to be integrated onto the BSim bench, currently under development by the same industrial partner. The dataset comprises 56 different optical surfaces, each with a relatively large clear aperture of (25 mm × 5 mm). For each map, several non-overlapping circular sub-apertures with a diameter of 2.24 mm were extracted. Zernike polynomials from index 4 to 36 were then fitted to these sub-apertures and used as inputs for the CNES simulation tool. An example of a measured surface error map, along with the extracted sub-apertures, is shown in figure 6. The typical root mean square wavefront error of a full 25×5 mm map is approximately 1 *nm*, corresponding to a surface quality on the order of $\lambda/1000$, and thus representative of very high-quality optical components. In a realistic scenario, the wavefront propagates through multiple optics, each contributing with its own wavefront error, before interfering with the reference beam at the detector.

To account for this, a simulation was implemented in which a WFE map is added to a flat–top beam with randomly selected sub-apertures from each of the 56 measured individual error maps. This process was repeated 1000 times to gain confidence on the result, as exploring the entire configuration space would not be possible with such a high number of combinations and not be useful as most of the Zernike distribution fitted from the optical surfaces exhibit the same overall shape. The resulting TTL coefficient reached a value of 1.07 μm rad^{-1} for the left/right actuation axis, and a slightly lower value was observed for the up/down axis. This asymmetry is attributed to anisotropy in the surface error distributions, likely induced by the manufacturing and polishing processes. For comparison with the randomly generated wavefront error maps using the exponentially decreasing Zernike weighting function, assuming the maps are uncorrelated, the total RMS surface error combines in quadrature:

$$\sigma_{\text{total}} = \sqrt{N_{\text{maps}}} \times \sigma_{\text{individual}}. \tag{6}$$

Using $N_{\text{maps}} = 56$ surfaces, each contributing an individual rms surface error of 1 nm, this yields a total wavefront error of $\sigma_{\text{total}} = 7.48$ nm, corresponding to approximately $\lambda/140$. The simulation done at $\lambda/140$ nm rms with the APC tool yields a $0.89 \pm 0.20\,\mu$m rad^{-1} coupling coefficient, in accordance with the simulation done with the real maps.

[8] The w_i weighting function in 3 is constant and equal to 1.

5. Conclusion

Optical aberrations are present in all optical systems, and defining maximum allowable RMS surface error values (either for individual components or the system as a whole) is a critical step to ensure that the instrument meets its performance requirements. The non-trivial and nonlinear relation between wavefront error and TTL coupling creates a challenge that cannot be addressed with simple analytical estimates. This motivated the development of dedicated simulation tools capable of evaluating the TTL impact of complex wavefront configurations. These tools provide essential guidance during the design and specification phases of optical instruments, enabling requirements to be set based on realistic scenarios rather than overly conservative margins. The two simulation tools developed in this study demonstrated good agreement across various physical scenarios, providing confidence in the reliability of the results. The analyses presented in this paper revealed that the coupling between wavefront aberrations and TTL is nonlinear when described through a Zernike decomposition, exhibiting non-homogeneous and non-additive behaviors. This nonlinearity induced the use of a large number of simulations across varying RMS amplitude levels to statistically capture the full range of possible coupling effects. The results indicate that achieving the required $15\,\mu\mathrm{m\,rad}^{-1}$ precision on the TTL coupling measurement for the OB Science Interferometer necessitates an overall output beam wavefront quality on the order of $\lambda/30$ RMS, including a 25% margin. Adding aberrations to the reference (non-tilted) beam led to an increase in the TTL coupling coefficient roughly by a factor of $\sqrt{2}$, consistent with expectations for the combination of two uncorrelated RMS error distributions. This result reinforces the validity of the $\lambda/30$ wavefront error requirement presentlyimposed on the interferometric beams to meet the TTL specification.

Acknowledgments

The authors acknowledge financial support from the Centre national d'études spatiales (CNES), France (ROR: https://ror.org/04h1h0y33), within the framework of the LISA space mission. The authors also thank E. Fitzsimmons, whose Fieldprop simulation library inspired part of the toolset used in this study.

Data availability statement

All data that support the findings of this study are included within the article (and any supplementary files).

ORCID iDs

Maxime Vincent 0009-0003-0888-4859
Romain Arguel 0009-0006-4002-9627
Hubert Halloin 0000-0002-9250-4622

References

[1] Amaro Seoane P *et al* 2017 Laser interferometer space antenna (arXiv:1702.00786)
[2] Colpi M *et al* 2023 ESA-SCI-DIR-RP-002 (arXiv:2402.07571)
[3] Armano M *et al* 2016 *Phys. Rev. Lett.* **116** 231101
[4] Robertson D I, McNamara P, Ward H and Hough J 1997 *Class. Quantum Grav.* **14** 1575–7
[5] Hartig M S, Schuster S and Wanner G 2022 *J. Opt.* **24** 065601
[6] Hartig M S, Schuster S, Heinzel G and Wanner G 2023 *J. Opt.* **25** 055601
[7] Chwalla M *et al* 2016 *Class. Quantum Grav.* **33** 245015
[8] Paczkowski S *et al* 2022 *Phys. Rev. D* **106** 042005
[9] Heinzel G, Álvarez M D, Pizzella A, Brause N and Delgado J J E 2020 *Phys. Rev. Appl.* **14** 054013
[10] Zernike F 1934 *Physica* **1** 689–704
[11] Cash W 2011 *Astrophys. J.* **738** 76
[12] Krist J 2007 Proper: an optical propagation library for idl *Proc. SPIE* **6675** 66700
[13] Goodman J W 1968 *Introduction to Fourier Optics* (McGraw-Hill)
[14] Noll R J 1976 *J. Opt. Soc. Am.* **66** 207–11
[15] Weaver A J, Mueller G and Fulda P J 2022 *Class. Quantum Grav.* **39** 195016
[16] Harrer S *et al* 2025 Validation of optical pathlength stability in a lisa test-bench demonstrator (arXiv:2511.16749)
[17] Gerberding O, Sheard B, Bykov I, Kullmann J, Delgado J J E, Danzmann K and Heinzel G 2013 *Class. Quantum Grav.* **30** 235029
[18] Schwarze T S, Fernández Barranco G, Penkert D, Kaufer M, Gerberding O and Heinzel G 2019 *Phys. Rev. Lett.* **122** 081104